Synthesis of porous hollow spheres Co@TiO 2-x - carbon composites for highly efficient lithium-ion batteries

Chunyong Liang
Fujian Provincial Collaborative Innovation Center for Ultra-Precision Optical Engineering and applications
Zhongliang Huang
Fujian Provincial Collaborative Innovation Center for Ultra-Precision Optical Engineering and applications
Lu Chen
Hebei University of Technology
Hongshui Wang
Hebei University of Technology
Tai Yang
Hebei University of Technology
Ning Liu (ningliu1985@hebut.edu.cn)
Hebei University of Technology
Tingdi Liao
Fujian Provincial Collaborative Innovation Center for Ultra-Precision Optical Engineering and applications
Feng Wang
Fujian Provincial Collaborative Innovation Center for Ultra-Precision Optical Engineering and applications

Research Article

Keywords: Lithium-ion batteries, Titanium dioxide, oxygen vacancies, chemical vapor deposition

Posted Date: April 8th, 2022

DOI: https://doi.org/10.21203/rs.3.rs-1520224/v1

Abstract

The hollow TiO_2 anode material has received great attention for next-generation LIBs because of its excellent stability, environmental friendly, and low volume change during lithiation/delithiation. Nevertheless, the current anatase TiO_2 anode materials are unable to be energy storage system owing to low lithium ion diffusivity and poor reversible theoretical capacities. The introduction of defects has been turned out to be a significant and effective method to improve electronic conductivity, especially oxygen vacancies (OVs). In this paper, a facile hydrothermal reaction and subsequent chemical vapor deposition method were successfully used to fabricate Co@TiO_{2-x}-carbon hollow nanospheres. These results suggest that the synthesized product exhibits good rate performance and superior cycling stability.

1. Introduction

Lithium-ion battery has high energy storage and long cycle life, so it has a great research and application value secondary battery field [1,2]. In general, graphite is used as the anode of the Lithium-ion battery. However, it has a relatively low theoretical gravimetric capacity, which cannot achieve the demand of LIBs industry for high theoretical capacity and energy density. Therefore, a variety of alternative anode materials have been widely studied [3-5]. Among all proposed candidates for the anode, TiO_2 has the advantages of high theoretical capacity, excellent Li-ion storage performances and environmental friendliness. In addition, the hollow nanospheres structure of TiO_2 provided a sufficient amount of space to inhibit the volume change effectively during the lithiation/delithiation process. Therefore, TiO_2 has a potential value in LIBs. However, the poor conductivity of TiO_2 causes the large initial impedance of TiO_2 anode, which seriously affects its rate performance [6-9]. In order to solve the inherent defect, different methods have been tried in recent years, including reducing particle size, doping elements, carbon coating, designing nanostructure morphology and introducing defects [10,11].

In these methods, the introduction of defects has been proved to be effective in improving electronic conductivity, especially in the production of OVs, which is self-modifying and easy to operate [12]. The methods of introducing OVs into TiO_2, including hot hydrogen, plasma, electrochemical and deoxidizer hydrothermal reductions reactions [13,14]. The introduction of nanostructures and conductive materials can also improve the electrochemical performance of TiO_2 anode [15,16]. The high specific surface of the hollow nanospheres structure can fast highways for lithium ion (Li^+) and improve the conductivity of LIBs. Moreover, the introduction of conductive materials can also improve the conductivity and buffer volume expansion during lithiation and delithiation. Both of them enhanced the electrochemical performances of the TiO_2 anode [17].

Inspired by this, we prepared Co@TiO_{2-x}-carbon hollow nanospheres by hydrothermal method and chemical vapor deposition (CVD) method to obtain excellent LIBs anode materials. Smooth conformal amorphous carbon with controllable thickness was deposited on the active material by CVD, which significantly improves the electrochemical performance of active materials. The optimized Co@TiO_{2-x}-

carbon composite has porous, rich defects and carbon coating properties. Carbon coating, metal cobalt and oxygen vacancies can increase the electrical conductivity of the materials, thus improving the rate performance; porous hollow nanospheres can provide more lithium storage sites, shorter Li^+ and electron diffusion path, at the same time, the appropriate internal cavity can inhibit the volume expansion during the cycle, so it has outstanding rate ability and cycling performance [18]. Consequently, the composite electrode presents a favorable rate performance with high current density (217 mAh g^{-1} at 1 A g^{-1}). Even after 1000 long cycles, a high capacity of 173 mAh g^{-1} at 1 A g^{-1} can also be achieved, which shows an excellent cycle performance.

2. Materials And Methods

2.1. Material Preparation

2.1.1. Synthesis of TiO_2

The TiO_2 microspheres were prepared through hydrothermal method and CVD method. $Ti(SO_4)_2{\cdot}9H_2O$ (0.81 g) was uniformly dissolved in anhydrous ethanol (75 ml) to form a homogeneous solution, denoted as solution A. Next, add 6 mL H_2O_2 and 0.43 g NH_4Cl to the above solution sequentially, followed by vigorous stirring, till complete dissolution (solution B). The obtained solution B was transferred to an autoclave, followed by a hydrothermal treatment in an oven at 120°C for 12 h. The white precipitated product was separated by centrifugation and washed with deionized water and absolute ethanol, subsequently dried in an oven.

2.1.2. Synthesis of Co@TiO_{2-x}-carbon composite

Firstly, 0.04 g $Co(NO_3)_2{\cdot}6H_2O$ materials were dissolved in the mixed solution B and then according to the above method, the CoO_x@TiO_2 material was obtained. The Co@TiO_{2-x}-carbon composite was synthesized by a subsequent annealed treatment. The as-formed CoO_x@TiO_2 composite was put in a ceramic boat and heated to 350 °C in the tube furnace under Ar atmosphere, and further heated to 560 °C under H_2 atmosphere; Finally, maintained at 560 °C in C_2H_2 atmosphere for 30 min. The synthesized sample was named as Co@TiO_{2-x}-carbon. Figure1 illustrates the flowchart for the preparation of the composite material.

2.2. Material Preparation

Phase compositions of samples were determined by X-ray diffraction (XRD) using Bruker D8 Discover diffractometer. Scanning electron and transmission electron microscopies (SEM and TEM) images were obtained by using Hitachi S-4800 and JEM 2100F (JEOL) instruments, respectively. The elemental analysis was performed using the Axis Ultra DLD spectrometer. The nitrogen adsorption-desorption isotherms and Brunauer-Emmett-Teller (BET) surface area were determined by the V-Sorb 2800P instrument.

2.3. Electrochemical measurements

At room temperature, a coin cell (CR2032) was used to conduct the electrochemical test with as-prepared materials as an anode. The as-prepared material, conductive agent super P and polyvinylidene fluoride (PVDF) were mixed with NMP at the mass ratio of 8:1:1 to obtain the slurry. Subsequently, the slurry was coated on a cuprum foil with a scraper, and then dried in a vacuum to form the electrode plate. The anode was obtained by punching a circle with a diameter of 12 cm. The semi battery is composed of anode electrode, electrolyte, separator and counter electrode. Cyclic voltammetry (CV) curves were recorded at 0.1 mV/s between 0.01 and 3.0 V via an electrochemical workstation (CHI760E). The charge/discharge curves of electrode material at different rate test was conducted with the voltage range from 0.01 to 3.0 V.

3. Results

To verify the crystalline structure of the synthesized products, the XRD patterns were presented in Fig. 2. The characteristic peaks at 25.3°, 37.8° and 48° correspond to (101), (004) and (200) planes of TiO_2 (PDF#78-2486), respectively, indicating that the synthesized products have a high crystalline nature. The wide peak of Co@TiO_{2-x}carbon at about 26.7° indicates the success of carbon coating [19]. In the figure no other impurities are detected, confirming that the as-prepared products have high purity. Therefore, XRD showed that Co@TiO_{2-x}-carbon and TiO_2 were successfully fabricated.

The characterization analysis about the basic morphological structure of Co@TiO_{2-x}-carbon nanoparticles was conducted by SEM. It is observed that the hollow composite possessed a nearly homogeneous spherical shape and a high dispersity. (Fig. 3a). The diameter of the nanospheres is about 800 nm. As shown in Fig. 3b, Ti, O, Co and C are uniformly dispersed on the nanospheres.

The SEM image reveals that the as-synthesized composite forms a hollow nanospheres structure in Fig. 4a. Meanwhile, the hollow morphology of the composite has been further described by the TEM images in Fig. 4f. The porous hollow spherical structure can provide more lithium storage sites, shorter lithium ion and electron diffusion paths. At the same time, the appropriate internal cavity can well adjust the structure and volume change of the electrode. The HRTEM of Fig. 4b shows the existence of cobalt metal and TiO_2. The existence of TiO_2 can be further clearly observed by FFT and inverse FFT transformation of Fig. 4c-e. The existence of Ti^{3+} and oxygen vacancies can facilitate the migration of electron of the materials, thus the composite electrode exhibits a superior rate performance. The linear scanning and corresponding element mapping of Fig. 4f show that TiO_2 and cobalt metal are uniformly distributed on the surface of hollow nanospheres.

A nitrogen adsorption experiment was used to test the pore characteristics of synthetic products, as shown in Fig. 5a. Compared with TiO_2 (67.4 m^2 g^{-1}), the composite possesses a high specific surface area which was about 190.8 m^2 g^{-1}. The N_2 adsorption-desorption isotherm curves of TiO_2 and Co@TiO_{2-x}-carbon belong to type-IV isotherm, indicating abundant mesopore structure (Fig. 5b). Co@TiO_{2-x}-carbon composite has a wide range of mesoporous size distribution, which is conducive to the transport of

lithium ions and can accommodate huge volume changes in the cycling process. Besides, the abundant mesoporous structure and large specific surface area provide more lithium insertion sites and voids to facilitate the storage of lithium and improve the rate ability and cycling performance of LIBs.

Electrochemical properties of the anode materials were further studied, as shown in Fig. 6, the lithium storage capacity was evaluated by half cells and prepared electrode. Due to the lithiation/delithiation effect of the carbon phase, the range (0.01-3 V) can lead to higher reversible capacity.

The lithium storage behaviors of the synthesized samples were investigated in half cells at a scanning rate of 0.1 mV s^{-1} and in a scanning range of 0.01-3 V. The curves show the initial five cycles of the as-prepared products are shown in Figure 6a and 6c. The first small reduction peak of the composite at 1.75 V during the first discharge can be attributed to the insertion of Li^+ into TiO_2 to form $Li_{0.5}TiO_2$ (The inset images in Fig. 6a). As we all known, due to the existence of TiO_{2-x}, the conductivity of Li_xTiO_2 formed in situ is also improved [20,21]. Meanwhile, in subsequent cycles, the reduction/oxidation peak of 1.50/1.70 can be attributed to TiO_{2-x} and the reduction/oxidation peak of 1.75/2.02 can be attributed to TiO_2 [22]. The CV curves of TiO_2 sample displays one oxidation peak at approximately 2.10 V and a reduction peak at approximately 1.70 V, which are in agreement with anatase TiO_2 (Fig. 6c) [23].

Discharge/charge profiles of lithium-ion battery with two samples are exhibited in Fig. 6b, d at 0.2 A g^{-1} under a voltage window of 0.01-3 V. The first discharge capacity of the composite electrode is 323 mAh g^{-1}, superior to TiO_2 electrode (214 mAh g^{-1}). Simultaneously, the result of the first cycle shows that the composite electrode exhibits low initial coulomb efficiency (ICE), which may be associated with the construction of a solid electrolyte interface (SEI) membrane [24]. Furthermore, the complex anode delivers a discharge specific capacity of 302 mAh g^{-1} in the following cycle, whereas TiO_2 electrode in the same process only 209 mAh g^{-1}. Compared with TiO_2 electrode, the charge-discharge curve of the composite electrode shows a similar and clear potential platform and is stable, which reveals the prominent reversibility of electrochemical reactions for the composite anode [25].

As shown in Fig. 6e, Co@TiO_{2-x}-carbon provides the highest discharge specific capacity during the test at 0.2 A g^{-1}. After 100 cycles, the composite material delivers a higher reversible capacity of 242 mAh g^{-1} than TiO_2 nanoparticles (139 mAh g^{-1}), demonstrating that the composite material possesses an outstanding reversibility [26]. The introduction of the carbon layer can increase the capacity of LIBs. In addition, the design of porous hollow nanospheres, the introduction of oxygen vacancies and metal cobalt can promote cycle stability.

The rate capability of the electrodes is further compared in Fig. 6f. Compared with TiO_2, the electrochemical performance of the composite electrode has a higher reversible capacity and better cycling performance at different current densities. The discharge capacities under the conditions of 0.1, 0.2, 0.5 and 1 A g^{-1} were 379, 291, 253 and 217 mAh g^{-1}, respectively. Electron conductivity and diffusion path determine the rate performance of LIBs [27,28]. The structure of hollow nanospheres of the

Co@TiO_{2-x}-carbon shortens the diffusion path of Li^+ and electron, and the existence of VOs, carbon coating and cobalt metal improve the conductivity essentially.

It is worth noting that Co@TiO_{2-x}-carbon exhibits strong cycle stability (no significant capacity degradation and close to 100% coulombic efficiency) at a high current density at 1 A g^{-1} and maintains 173 mAh g^{-1} after 1000 cycles. Obviously, the composite electrode displays much better cycle performance than TiO_2, and the reversible specific capacity of the composite material is much higher than that of TiO_2 (42 mAh g^{-1} at the 1000 th cycle) in Fig. 6g. Due to the specific hollow structure of the as-prepared product, which can inhibit the volume expansion during the cycling process and obtain excellent cycling performance.

Fig. 6h shows the EIS of anode materials. The two Nyquist plots are both consisted of a compressed semicircle at the high-frequency region followed by a sloping line in the low frequency region. The low-frequency region represents the Warburg diffusion process which might be attributed to the diffusion of the lithium ions, and the semicircle at high frequency corresponds to the charge-transfer resistance [29]. Clearly, the composite has lower resistance and better conductivity than the TiO_2 sample, which are caused by the Li-ion insertion/extraction rates. Therefore, the composite product exhibits superior electrochemical reaction kinetics.

4. Conclusions

In summary, a simple hydrothermal and CVD method was used to synthesize Co@TiO_{2-x}-carbon hollow nanospheres. The addition of OVs, Co metal and carbon layer improves the electrical conductivity of the synthesis product to a certain extent, thus exhibiting a remarkable rate performance of the composite. Hollow nanospheres have rich pore size, provide more lithium storage sites, shorter lithium ion and electron diffusion path. At the same time, the appropriate cavity structure can better inhibit the volume change during the cycle, and significantly improve the cycle stability. The results show that Co@TiO_{2-x}-carbon hollow nanospheres are promising materials for advanced anode materials of LIBs.

Declarations

Ethics approval and consent to participate: Not applicable.

Consent for publication: All authors approve the manuscript for publication.

Availability of data and material: All data generated or analysed during this study are included in this published article

Competing interests: The authors declare that they have no competing interests.

Funding: This research was funded by the Science and Technology Major Special Project of Fujian Province (2021HZ021027).

Authors' contributions: C.L. and Z.H. wrote the main manuscript text. L.C., H.W. and T.Y. prepared figures. All authors read and approved the final manuscript.

Acknowledgements: Not applicable.

References

1. Wang, Y.; Chen, L.J.; Pan, D.; Guo, Z.H.; Xia, S.B. Porous TiO_2–$FeTiO_3$@Carbon nanocomposites as anode for high-performance lithium-ion batteries. *J. Alloy. Compd*. **2020**, *858*, 157635.
2. Zhang, Y.; Zhao, Y.; Bakenov, Z.; Tuiyebayeva, M.; Konarov, A.; Chen, P. Synthesis of Hierarchical Porous Sulfur/ Polypyrrole/Multiwalled Carbon Nanotube Composite Cathode for Lithium Batteries. *Electrochim. Acta* **2014**, *143*, 49-55.
3. Zhang, P.; Liu, Y.; Zhou, M.; et al. Rational designed C/Co_9S_8@SnS_2 nanocomposite as a highly efficient anode for lithium ion batteries. *Nanotechnology* **2020**, *31,* 395401.
4. Jing, W.; Zhang, P.L.; Liu, J.Z.; Zhou, C.C.; Guo, S.Z.; Li, S.; Lei, Y.C.; Li, K.; Chen, L.Y. Control Synthesis of N-Doped Carbon and TiO_2 Double-Shelled Nanospheres with Encapsulated Multi-Layer MoO_3 Nanosheets as Anode for Reversible Lithium Storage. *Dalton Trans.* **2020**, *49*, 10928-10938.
5. Han, Q.J.; Sheng, Y.L.; Han, Z.W.; Li, X.; Zhang, W.Q.; Li, Y.; Zhang, X. Metallic Sb nanoparticles embedded into yolk-shell Sb_2O_3@TiO_2 composite as anode materials for lithium ion batteries. *New J. Chem.* **2020**, *44*.
6. Zhen, M.M; Guo, S.Q.; Li, K.F.; Li, H.A.; Shen, B.X. Template-free construction of hollow TiO_2 microspheres for long-life and high-capacity lithium storage. *J. Alloy. Compd*. **2020**, *859*, 157761.
7. Jiang, W.W.; Liu, Q.H.; Peng, J.F.; Jiang, Y.H.; Ding, Y.H.; Wei, Q. Co_9S_8 nanoparticles embedded into amorphous carbon as anode materials for lithium-ion batteries. *Nanotechnology* **2020**, *31,* 235713.
8. Bae, J.; Han H.; Kim, Y.; et al. Surfactant-Controlled synthesis of polygonal-stacked Cu_2O for morphology effect on lithium-ion battery anode performance. *J. Phys. Chem. Solids* **2020**, *150*, 109849.
9. Gong, Q.H.; Wang, H.Q.; Song, W.H.; et al. Front Cover: Tunable Synthesis of Hierarchical Yolk/Double-Shelled SiO_x@TiO_2@C Nanospheres for High-Performance Lithium-Ion Batteries. *Chem. Eur. J.* **2021**, *27*, 2555-2555.
10. Wang, P.; Zhang, G.; Cheng, J.; You, Y.; Li, Y.K.; Ding, C.; Gu, J.J.; Zheng, X.S.; Zhang, C.F.; Cao, F.F. Facile Synthesis of Carbon-Coated Spinel $Li_4Ti_5O_{12}$/Rutile-TiO_2 Composites as an Improved Anode Material in Full Lithium-Ion Batteries with $LiFePO_4$@N-Doped Carbon Cathode. *ACS Appl. Mater. Interfaces* **2017,** *9,* 6138-6143.
11. Liu, H.; Li, W.; Shen, D.K.; Zhao, D.Y.; Wang, G.X. Graphitic Carbon Conformal Coating of Mesoporous TiO_2 Hollow Spheres for High-Performance Lithium Ion Battery Anodes. *J. Am. Chem. Soc.* **2015,** *137,* 13161-13166.

12. Zhang, Y.; Xing, Z.P.; Liu, X.F.; Li, Z.Z.; Wu, X.Y.; Jiang, J.J.; Li, M.; Zhu, Q.; Zhou, W. Ti^{3+} Self-Doped Blue TiO_2(B) Single-Crystalline Nanorods for Efficient Solar-Driven Photocatalytic Performance. *ACS Appl. Mater. Interfaces* **2016,** *8,* 26851-26859.
13. Li, J.L.; Zhang, M.; Guan, Z.J.; Li, Q.Y.; Yang, J.J. Synergistic Effect of Surface and Bulk Single-Electron-Trapped Oxygen Vacancy of TiO_2 in the Photocatalytic Reduction of CO_2. *Appl. Catal. B Environ.* **2017,** *206,* 300-307.
14. Li, Z.; Ding, Y.T.; Kang, W.J.; Li, C.; Lin, D.; Wang, X.Y.; Chen, Z.W.; Wu, M.H.; Pan, D.Y. Reduction Mechanism and Capacitive Properties of Highly Electrochemically Reduced TiO_2 Nanotube Arrays. *Electrochim. Acta* **2015,** *161,* 40-47.
15. Jung, M.H. Carbon-Coated ZnO Mat Passivation by Atomic-Layer-Deposited HfO_2 as an Anode Material for Lithium-Ion Batteries. *J. Colloid Interf. Sci.* **2017,** *505,* 631-641.
16. Tu, Z.M.; Yang, G.Z.; Song, H.W.; Wang, C.X. Amorphous ZnO Quantum Dot/Mesoporous Carbon Bubble Composites for a High-Performance Lithium-Ion Battery Anode. *ACS Appl. Mater. Interfaces* **2016,** *9,* 439-446
17. Ashuri, M.; He, Q.; Shaw, L.L. Improving cycle stability of Si anode through partially carbonized polydopamine coating. *J. Electroanal. Chem.* **2020**, *876*, 114738.
18. Zhang, Y.; Zhao, Y.; Konarov, A.; Li, Z.; Chen, P. Effect of mesoporous carbon microtube prepared by carbonizing the poplar catkin on sulfur cathode performance in Li/S batteries, *J. Alloy. Compd.* **2015**, *619*, 298-302.
19. Tian, Y.; Zhao, Y.; Zhang, Y.; Ricardez-Sandoval, L.; Wang, X.; Li, J. Construction of Oxygen-Deficient La(OH)3 Nanorods Wrapped by Reduced Graphene Oxide for Polysulfide Trapping toward High-Performance Lithium/Sulfur Batteries. *ACS Appl. Mater. Interfaces* **2019**, *11*, 23271-23279.
20. Wu, N.T.; Qiao, X.G.; Shen, J.K.; Liu, G.L.; Sun, T. Wu, H.; Hou, H.S.; Liu, S.M.; Zhang. Y.; Ji, X.B. Anatase Inverse Opal TiO_{2-X}@N-doped C induced the Dominant Pseudocapacitive Effect for Durable and Fast Lithium/Sodium Storage. *Electrochim. Acta* **2019,** *299,* 540-548.
21. Jeong, G; Kim, J.G.; Park, M.S.; Hwang, S.M.; Kim, Y.U.; Kim, Y.J.; Kim, J.H.; Dou. S.X. Core-Shell Structured Silicon Nanoparticles@TiO_{2-X}/Carbon Mesoporous Microfiber Composite as a Safe and High-Performance Lithium-Ion Battery Anode. *ACS Nano* **2014,** *8,* 2977.
22. Huo, J.H.; Xue, Y.X.; Zhang, L.F.; Wang, X.F.; Cheng, Y.Q.; Guo, S.W. Hierarchical TiO_{2-X} Nanoarchitectures on Ti Foils as Binder-Free Anodes for Hybrid Li-ion Capacitors. *J. Colloid Interface Sci.* **2019,** *555,* 791-800.
23. Kang, S.H.; Jo, Y.N.; Prasanna, K.; Santhoshkumar, P.; Joe, Y.C.; Vediappan, K.; Lee, C.W. Bandgap Tuned and Oxygen Vacant TiO_{2-X} Anode Materials with Enhanced Electrochemical Properties for Lithium Ion Batteries. *J. Ind. Eng. Chem.* **2018,** *18,* 31382.
24. Deng, X.L.; Wei, Z.X.; Cui, C.Y.; Liu, Q.H.; Wang, C.Y.; Ma, J.M. Oxygen-Deficient Anatase TiO_2@C Nanospindles with Pseudocapacitive Contribution for Enhancing Lithium Storage. *J. Mater. Chem. A* **2018,** *6,* 4013-4022.

25. Zhang, J.; Li, G.; Zhang, Y.; Zhang, W.; Wang, X.; Zhao, Y.; Li, J.; Chen, Z. Vertically rooting multifunctional tentacles on carbon scaffold as efficient polysulfide barrier toward superior lithium-sulfur batteries. *Nano Energy* **2019,** *64*, 103905.
26. Li, H.; Sun, L.; Zhang, Y.; Tan, T.; Wang, G.; Bakenov, Z. Enhanced cycle performance of Li/S battery with the reduced graphene oxide/activated carbon functional interlayer, *J. Energy Chem.* **2017**, *26*, 1276-1281.
27. Zhao, Y.; Wang, L.P.; Sougrati, M.T.; Feng, Z.; Leconte, Y.; Fisher, A.; Srinivasan, M.; Xu, Z. A Review on Design Strategies for Carbon Based Metal Oxides and Sulfides Nanocomposites for High Performance Li and Na Ion Battery Anodes. *Adv. Energy Mater.* **2017,** *7,* 1601424.
28. Deng, M.X.; Li, S.J.; Hong, W.W.; Jiang, Y.L.; Xu, W.; Shuai, H.L.; Zou, G.Q.; Hu, Y.C.; Hou, H.S.; Wang, W.L.; Ji, X.B. Octahedral Sb_2O_3 as High-Performance Anode for Lithium and Sodium Storage. *Mater. Chem. Phys.* **2019,** *223,* 46-52.
29. Li, H.P.; Li, Y.; Zhang, Y.G.; Zhang, C.W. Facile synthesis of carbon-coated Fe3O4 core–shell nanoparticles as anode materials for lithium-ion batteries. *J. Nanopart. Res.* **2015**, *17*, 370.

Figures

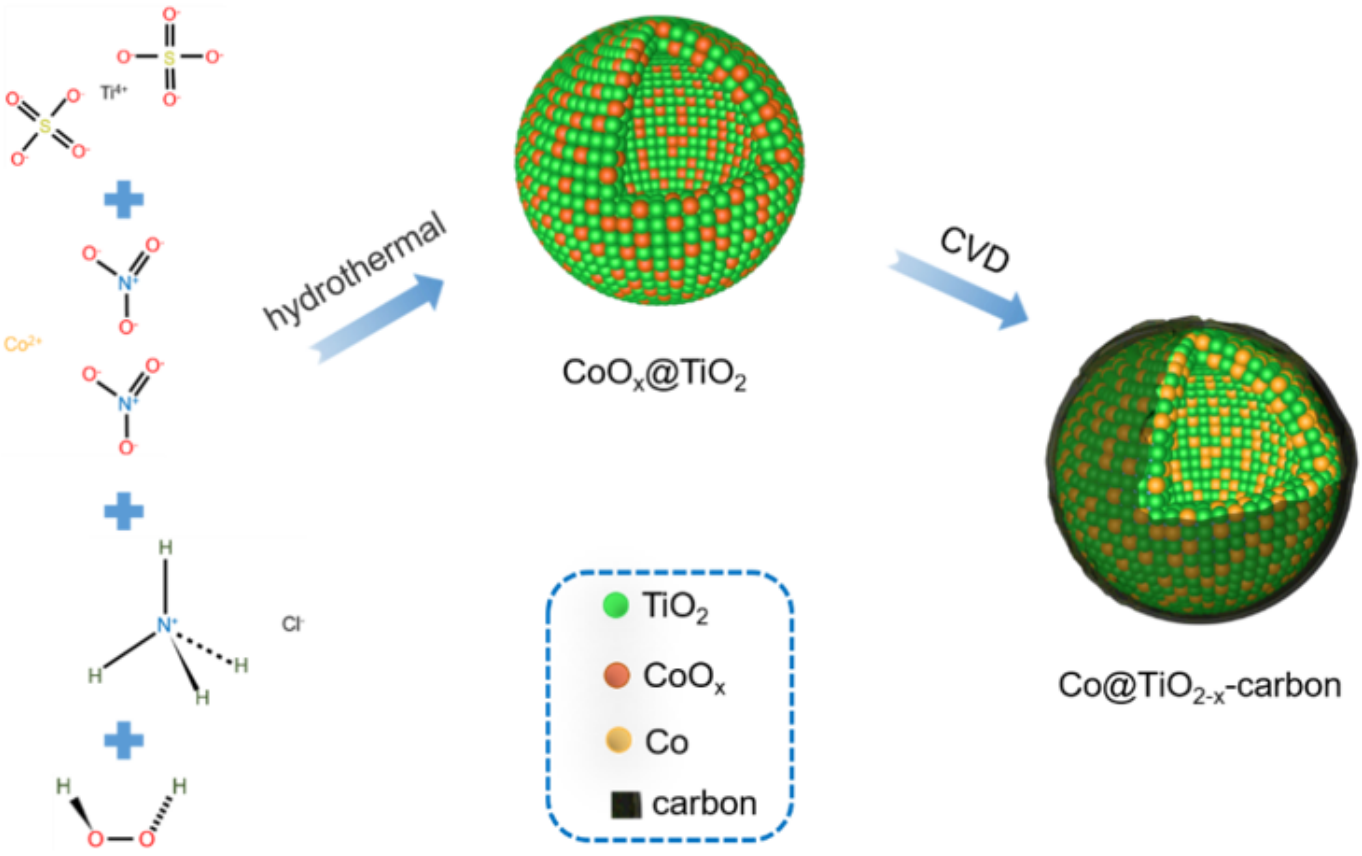

Figure 1

Synthesis strategy of hollow $Co@TiO_{2-x}$-carbon composite.

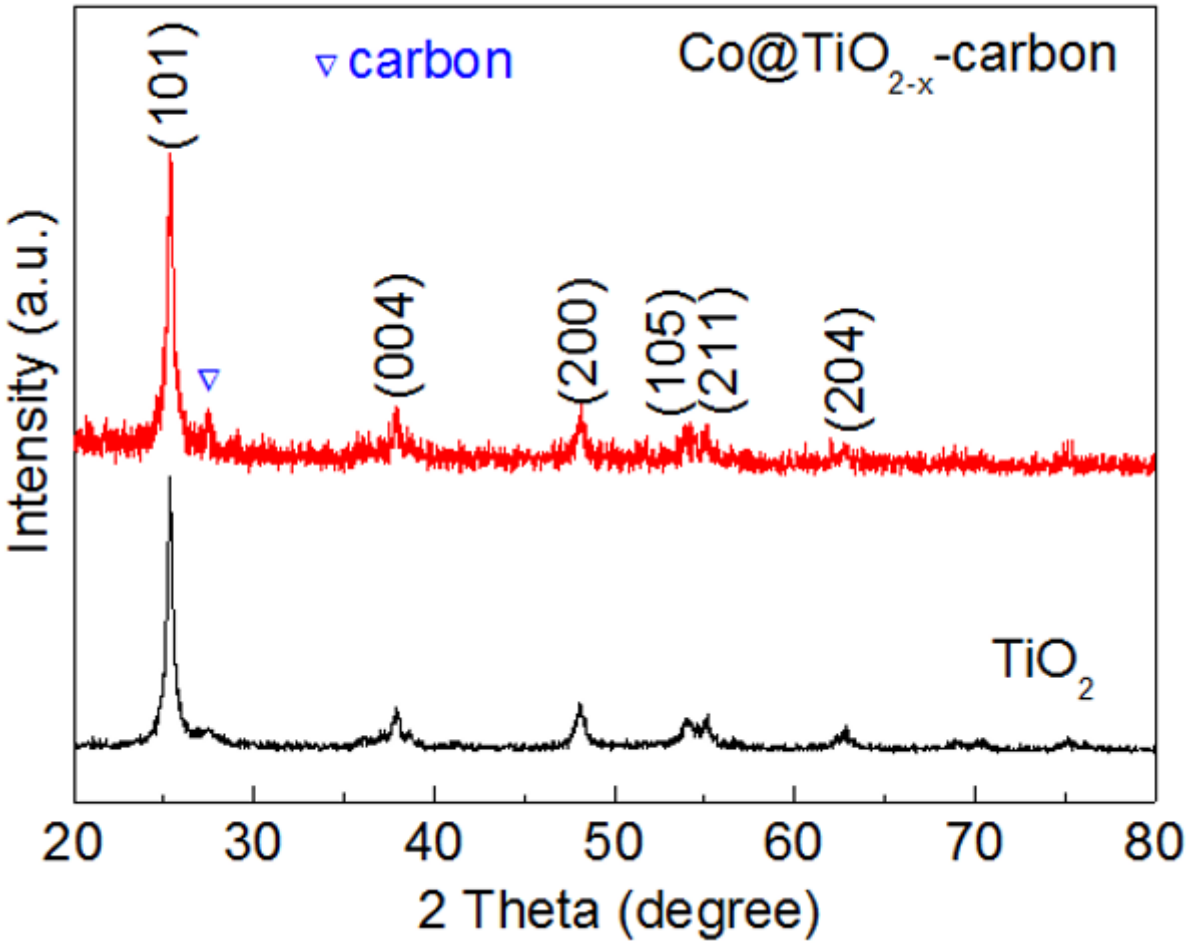

Figure 2

XRD pattern of the synthesized samples.

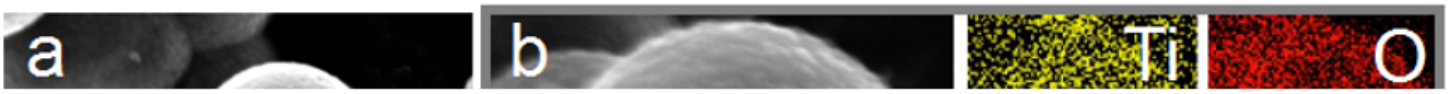

Figure 3

(a) SEM image; (b) high-resolution SEM image and corresponding EDS mappings of $Co@TiO_{2-x}$-carbon.

Figure 4

(a) SEM; (b) high-resolution TEM image; (c) FFT pattern; (d) the inverse FFT crystalline lattice image; (e) the lattice spacing profiles at selected areas in yellow and red; (f) linear scan and corresponding elemental mappings of Co@TiO_{2-x}-carbon.

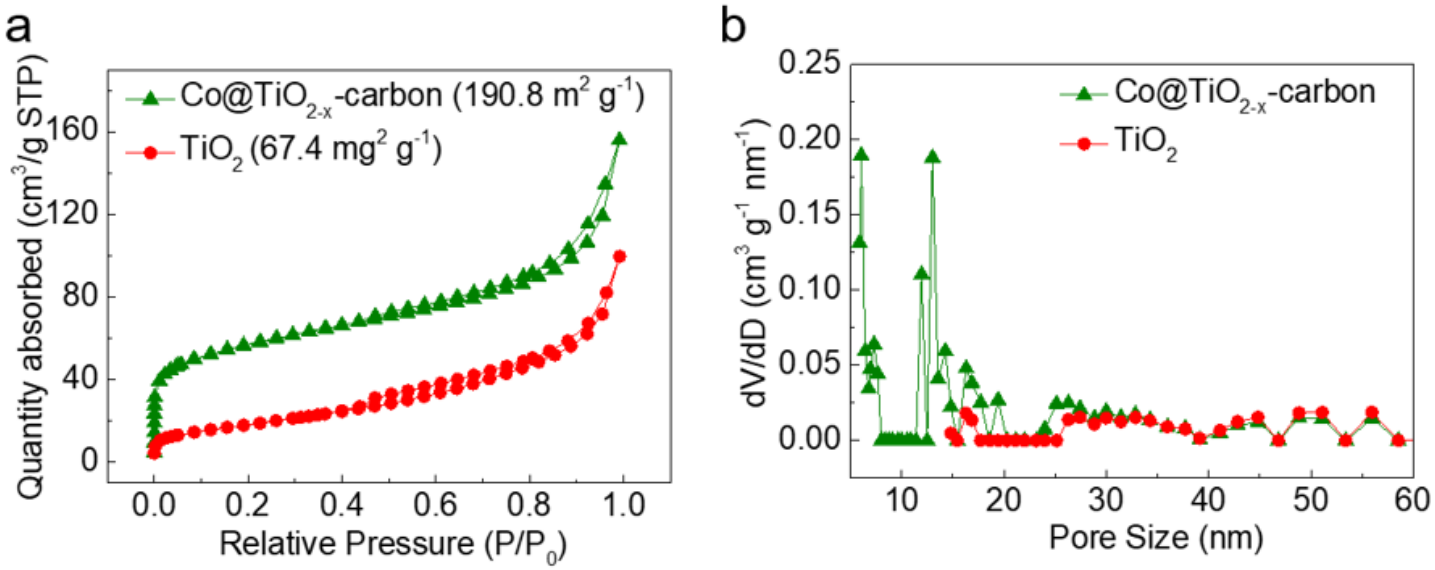

Figure 5

(a) N_2 adsorption-desorption isotherms and (b) pore size distributions of samples.

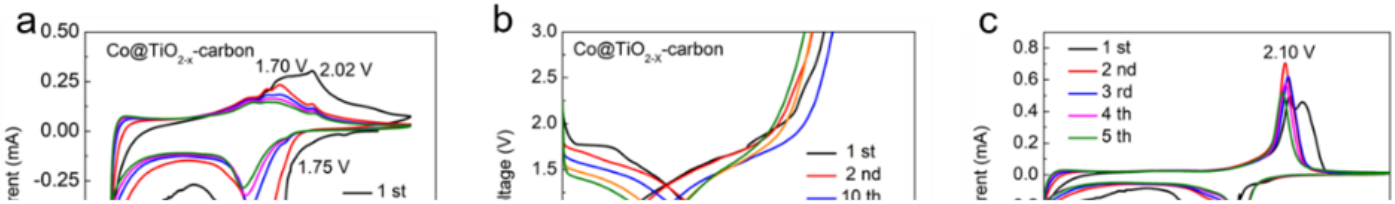

Figure 6

CV curves of (a) Co@TiO_{2-x}-carbon and (c) TiO_2; Charge-discharge voltage profiles of (b) Co@TiO_{2-x}-carbon and (d) TiO_2 at 0.2 A g^{-1}; (e) Cyclic stability and (f) rate capabilities of as-synthesized products; (g) Long cycling performance of as-synthesized products at 1 A g^{-1}; (h) Nyquist plots of as-synthesized products before cycling.